Acta Oceanol. Sin., 2018, Vol. 37, No. 7, P. 78–84
DOI: 10.1007/s13131-017-1246-9
http://www.hyxb.org.cn
E-mail: hyxbe@263.net

High-resolution bottom detection algorithm for a multibeam echo-sounder system with a U-shaped array

JIANG Ying[1, 2], YANG Zhiguo[3]*, LIU Zongwei[1, 2], YANG Chunmei[1, 2]

[1] Key Laboratory of Marine Science and Numerical Modeling, The First Institute of Oceanography, State Oceanic Administration, Qingdao 266061, China

[2] Laboratory for Regional Oceanography and Numerical Modeling, Qingdao National Laboratory for Marine Science and Technology, Qingdao 266237, China

[3] China National Deep Sea Center, State Oceanic Administration, Qingdao 266237, China

Received 25 August 2017; accepted 10 October 2017

Abstract

High-resolution approaches such as multiple signal classification and estimation of signal parameters via rotational invariance techniques (ESPRIT) are currently employed widely in multibeam echo-sounder (MBES) systems for sea floor bathymetry, where a uniform line array is also required. However, due to the requirements in terms of the system coverage/resolution and installation space constraints, an MBES system usually employs a receiving array with a special shape, which means that high-resolution algorithms cannot be applied directly. In addition, the short-term stationary echo signals make it difficult to estimate the covariance matrix required by the high-resolution approaches, which further increases the complexity when applying the high-resolution algorithms in the MBES systems. The ESPRIT with multiple-angle subarray beamforming is employed to reduce the requirements in terms of the signal-to-noise ratio, number of snapshots, and computational effort. The simulations show that the new processing method can provide better fine-structure resolution. Then a high-resolution bottom detection (HRBD) algorithm is developed by combining the new processing method with virtual array transformation. The application of the HRBD algorithm to a U-shaped array is also discuss. The computer simulations and experimental data processing results verify the effectiveness of the proposed algorithm.

Key words: high-resolution bottom detection, multibeam echo-sounder, subarray beamforming, virtual array transformation

Citation: Jiang Ying, Yang Zhiguo, Liu Zongwei, Yang Chunmei. 2018. High-resolution bottom detection algorithm for a multibeam echo-sounder system with a U-shaped array. Acta Oceanologica Sinica, 37(7): 78–84, doi: 10.1007/s13131-017-1246-9

1 Introduction

Bottom topography information forms the foundation of numerous human ocean activities, including marine environmental investigation, resource exploitation, and navigation security. The aim of a bathymetry measurement system is to measure the water depth and map the seabed topography. A multibeam echo-sounder (MBES) is a high-tech instrument that can obtain high-density strip depth measurements by exploiting wide-swath directional transmitting and multi-channel receiving. During the past 50 years, the MBES technology has been enhanced significantly and it continues to improve toward even wider swath coverage, higher resolution, and better precision. A major problem with these systems is that the footprint of a beam spreads gradually when steered away from the normal direction and severe resolution degradation occurs when it is integrated with the weakened strength of bottom backscattering signals at small grazing angles.

The depth of a measuring point on the bottom is determined by estimating the direction of arrival (DOA) and time of arrival (TOA). The DOA can be estimated from the beam angles, but the broadening footprints of outer inclined beams will reduce the resolution significantly and affect the depth estimation accuracy. In fact, the topographic relief within the footprint of an inclined beam makes the echo signals exhibit point-like features. Hence, high-resolution algorithms such as multiple signal classification and estimation of signal parameters via rotational invariance techniques (ESPRIT) (Roy and Kailath, 1989) can be used to distinguish the echo signals that arrive simultaneously from different directions to obtain sub-beamwidth resolution. New bottom detection methods using multiple subarrays (Yang and Taxt, 1997) have been proposed to estimate the DOA of bottom echoes with oblique incident angles. The mutual information between two close beams (Llort and Sintes, 2004) can be used to reconstruct the sea floor more accurately. Owing to the reduced side-lobe levels in the beam-array pattern, a precise and unambiguous bottom detection method was proposed for Simrad ME70 (Bourguignon et al., 2009).

However, considering the coverage/resolution requirements and installation space constraints, an MBES system usually employs a receiving array with a special shape, which means that the high-resolution algorithms are not suitable, where a uniform linear array (ULA) is a precondition. Short-term stationary echo signals also make it difficult to estimate the required covariance matrix, which further increases the complexity when applying

Foundation item: The National Natural Science Foundation of China under contract No. 41706066; the National Key R&D Program of China under contract No. 2016YFC1400200; the China-ASEAN Maritime Cooperation Fund.
*Corresponding author, E-mail: zg.yang@163.com

the high-resolution algorithms in the MBES systems.

The ESPRIT with multiple-angle subarray beamforming (Xu et al., 2012) was developed for an array with many array elements. This method can resolve more than one source direction in a beam with a few independent snapshots, which is beneficial for detecting the bottom echoes from areas with much rise and fall, and echoes with the oblique incident angles. However, this method can only estimate the DOA and it needs adjustments for bottom detection. The assumption of a linear receiving array in this method also limits the application of this method in the MBES systems.

Thus, in this study, we developed a high-resolution bottom detection algorithm (HRBD), which can be used on a planar array with any shape, by combining the ESPRIT with multiple-angle subarray beamforming and virtual array transformation. We also developed a special virtual transformation for a U-shaped array. The computer simulations and experimental data processing results show that compared with traditional bottom detection algorithms such as the bearing deviation indicator (BDI), the proposed algorithm can provide better fine-structure resolution.

This paper is divided into five sections, the first of which is the introduction. The second section briefly introduces the system. The third section describes the signal processing techniques employed in the HRBD. The fourth section presents the results of the computer simulations and experimental data processing results. In the fifth section, we summarize the results and give our conclusions and suggestions for future research.

2 System

A shallow-water MBES system (Jiang, 2011) is funded by the national 863 program as a research platform. This system employs U-shaped arrays, with transmitting and receiving conformal designs, as shown in Fig. 1. The system covers a 172° swath perpendicular to the ship's direction of movement (across-track). The main technical performance index parameters are shown in Table 1.

To considering rolling correction processing, the system forms 290 uniform receiving beams spanning from –85° to 85°, and the beam width is less than 1.5° (across-track).

3 Signal processing techniques

In the following, we present the methods for the ESPRIT with multiple-angle subarray beamforming (Xu et al., 2012; Jiang, 2011) and virtual array transformation for an U-shaped array (Jiang, 2011; Friedlander and Weiss, 1992; Weiss and Gavish, 1991). The implementation of the HRBD in the MBES system is then summarized.

3.1 *ESPRIT with multiple-angle subarray beamforming*

We assume that K uncorrelated far field narrowband sources impinge on a linear array of M equally spaced sensors with

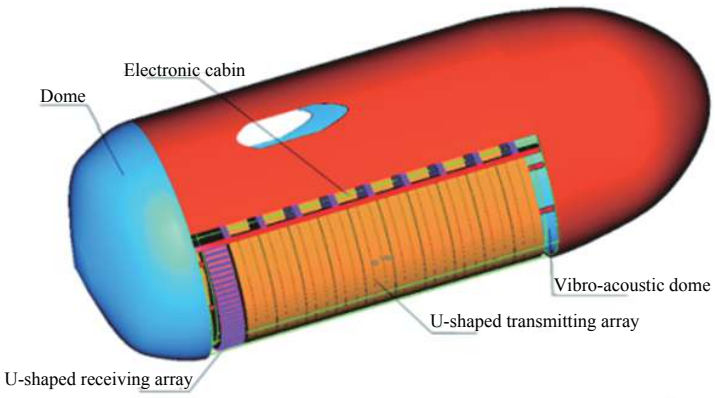

Fig. 1. Structure of the MBES system.

Table 1. Main technical performance index parameters for the MBES system

Parameter	Index parameter
Working frequency	165/195 kHz signal or dual frequency operation mode
Transmit pulse length	0.1–4 ms total five kinds
Transmit cycle	50–800 ms total four kinds
Array size	transmitting array: 300 mm (along-track) receiving array: 30 mm (along-track) 128 sensors of U-shaped array
Transmit beam width	1.5°×172° (along-track by across-track)
Maximum emission source level	215 dB
Receiving beam width	20°×1.5° (along-track by across-track)
Depth range (H)	1–200 m
Swath range (S_w)	1. $S_w \geqslant 8H$ (H: 1–100 m) 2. $S_w \geqslant 4H$ (H: 101–200 m)
Receiving beam number	256
Motion compensation	±10° rolling correction, ±10° pitch correction
Depth accuracy	10 cm plus or minus 0.5% depth range

sensor spacing d, which is less than or equal to half the wavelength. The $M \times 1$ received signal vector can be expressed as

$$\boldsymbol{x}(t) = \boldsymbol{A}\boldsymbol{s}(t) + \boldsymbol{n}(t), \tag{1}$$

where $\boldsymbol{s}(t) = [\ s_1(t) \quad \ldots \quad s_k(t)\ ]^{\mathrm{T}}$, $s_k(t)$ is the incident signal from the kth source, $(\cdot)^{\mathrm{T}}$ denotes the transpose; $\boldsymbol{A}$= $[\boldsymbol{a}(\theta_1)$ ... $\boldsymbol{a}(\theta_k)\ ]$, $\boldsymbol{a}(\theta_k)$ is the array manifold vector, θ_k denotes the signal arriving from the direction of the kth source; and $\boldsymbol{n}(t)$ denotes the noise vector. For plane wave propagation, we have

$$\boldsymbol{a}(\theta_k) = [\ 1 \quad \mathrm{e}^{\mathrm{j}2\pi d \sin\theta_k/\lambda} \quad \ldots \quad \mathrm{e}^{\mathrm{j}2\pi(M-1)d\sin\theta_k/\lambda}\ ]^{\mathrm{T}}, \tag{2}$$

where λ is the wavelength. If we suppose that the noise is zero-mean white Gaussian with variance σ_n^2 and uncorrelated with the source signals, then the covariance of the received signal vector is

$$\boldsymbol{R}_{xx} = \boldsymbol{A}\boldsymbol{R}_{ss}\boldsymbol{A}^{\mathrm{H}} + \sigma_n^2\boldsymbol{I}_M, \tag{3}$$

where $\boldsymbol{I}_M$ denotes an $M \times M$ identity matrix, $(\cdot)^{\mathrm{H}}$ denotes the complex conjugate transpose; and $\boldsymbol{R}_{ss}$ is the source covariance matrix of rank K. Estimating the covariance requires sufficient statistical samples of both the signals and noise, which is particularly demanding when the number of sensors is large. In addition, the computational complexity is related to the number of sensors.

First, we divide the entire array into N identical subarrays, each with P sensors that are equally separated by D, which is an integer multiple of the sensor spacing. We denote the set of L beam pointing angles as $\bar{\theta}_l,\ l = 1, \ldots, L$. The ESPRIT method with multiple-angle subarray beamforming can then be applied.

The commonly used total least squares (TLS) version of ESPRIT with multiple-angle subarray beamforming is denoted as TLS-ESPRIT-SB and its implementation can be summarized as follows (Jiang, 2011).

(1) Divide the entire array into N identical subarrays, each with P sensors that are equally separated by D, and obtain the signal received $\boldsymbol{x}_i(t),\ i = 1, \ldots, N$ by each subarray. We denote a set of L beam pointing angles as $\bar{\theta}_l,\ l = 1, \ldots, L$.

(2) Obtain the beamforming outputs $\boldsymbol{y}_i(t),\ i = 1, \ldots, N$ from each subarray, and compute $\boldsymbol{z}(t) = [\ \boldsymbol{y}_1^{\mathrm{T}}(t) \quad \ldots, \quad \boldsymbol{y}_N^{\mathrm{T}}(t)\ ]^{\mathrm{T}}$.

(3) Obtain the sample covariance $\hat{\boldsymbol{R}}_{zz}$ as an estimate of $\boldsymbol{R}_{zz}$.

(4) Compute the eigendecomposition of $\hat{\boldsymbol{R}}_{zz}$ as

$$\hat{\boldsymbol{R}}_{zz} = \hat{\boldsymbol{E}}\hat{\boldsymbol{\Lambda}}\hat{\boldsymbol{E}}^{\mathrm{H}}. \tag{4}$$

(5) If necessary, estimate the number of sources K.

(6) Partition $\hat{\boldsymbol{E}}$= $[\hat{\boldsymbol{E}}_s|\hat{\boldsymbol{E}}_n]$, where $\hat{\boldsymbol{E}}_s$ are the principal eigenvectors corresponding to the K largest eigenvalues.

(7) Compute the eigendecomposition of the $2K \times 2K$ matrix as

$$\begin{bmatrix} \hat{\boldsymbol{E}}_{z_1}^{\mathrm{H}} \\ \hat{\boldsymbol{E}}_{z_2}^{\mathrm{H}} \end{bmatrix} \left[\hat{\boldsymbol{E}}_{z_1}\ \hat{\boldsymbol{E}}_{z_2}\right] = \boldsymbol{E}\boldsymbol{\Lambda}\boldsymbol{E}^{\mathrm{H}}, \tag{5}$$

where $\hat{\boldsymbol{E}}_{z_1}$ and $\hat{\boldsymbol{E}}_{z_2}$ pick the first and last $L(N-1)$ rows of $\hat{\boldsymbol{E}}_s$, respectively.

(8) Partition $\boldsymbol{E}$ into $K \times K$ submatrices, as follows:

$$\boldsymbol{E} = \begin{bmatrix} \boldsymbol{E}_{11} & \boldsymbol{E}_{12} \\ \boldsymbol{E}_{21} & \boldsymbol{E}_{22} \end{bmatrix}. \tag{6}$$

(9) Calculate the eigenvalues γ_k of $-\boldsymbol{E}_{12}\boldsymbol{E}_{22}^{-1}$, then

$$\hat{\theta}_k = \sin^{-1}\left(-\frac{\lambda}{2\pi D} \cdot \arg\gamma_k\right), \tag{7}$$

where $\arg(\cdot)$ retrieves the angle information.

Note that a simple choice of $L = 2$ or 3 is often sufficient to improve the beamspace DOA estimation performance. The dimension in the beamspace can be far less than that in the element space, thereby reducing the computational complexity and decreasing the number of snapshots needed to obtain a statistically robust covariance estimate. Hence, for $L \ll P$, the ESPRIT-SB exhibits significant computational advantages compared with the original ESPRIT method.

In practical multibeam system applications, the above described method can be applied to the selected beams following conventional beamforming to generate beams at a set of pre-selected angles and for subsequent source signal detection at each beam.

3.2 *Virtual transformation for a U-shaped array*

3.2.1 *Virtual transformation*

The virtual transformation technique is employed, as described previously (Friedlander and Weiss, 1992; Weiss and Gavish, 1991). The first step involves dividing the field of view for the array into H sectors, where the size depends on the array geometry and the desired accuracy.

Next, a set of angles Q_h (the subscript h denotes the sector index, $h = 1, \ldots, H$) are selected for the design of the virtual array manifold for each sector. A typical number of 50–100 equidistant angles spanning each sector are used for the implementation of the virtual transformation. The virtual array selected is a ULA for the high resolution method. The real array manifold $\boldsymbol{A}_h$ and the virtual array manifold $\hat{\boldsymbol{A}}_h$ constructed are associated with the set Q_h.

A virtual transformation matrix $\boldsymbol{B}_h$ is then designed to satisfy the least squares requirement according to the following equation:

$$\boldsymbol{B}_h\boldsymbol{A}_h = \hat{\boldsymbol{A}}_h. \tag{8}$$

Thus, the formula for $\boldsymbol{B}_h$ can be expressed as follows:

$$\boldsymbol{B}_h = \left(\boldsymbol{A}_h\boldsymbol{A}_h^{\mathrm{H}}\right)^{-1}\boldsymbol{A}_h\hat{\boldsymbol{A}}_h^{\mathrm{H}}. \tag{9}$$

The size of $\boldsymbol{B}_h$ is determined by the sensor number in the real array. The accuracy of this transformation is examined by comparing the ratio of the Frobenius norms for $\hat{\boldsymbol{A}}_h - \boldsymbol{B}_h\boldsymbol{A}_h$ and $\hat{\boldsymbol{A}}_h$ (Bourguignon et al., 2009). The sector size should be reduced and the transformation coefficients must be recalculated.

The results obtained after the procedure outlined above comprise a set of transformation matrices $\{\boldsymbol{B}_h\}$, which are computed only once (off-line) for any given array. Given these transformation matrices, the data covariance can be calculated for the virtual ULA based on the corresponding matrix of the real array, which is needed for ESPRIT-type methods.

3.2.2 *Virtual transformation based on a U-shaped array*

The U-shaped array in the MBES system has M nondirectional sensors distributed evenly on a parabolic shape, as shown in Fig. 2. The origin of the coordinates is located in the center of the parabola. When the system scans over wide angles, not all of the sensors can receive signals from some directions because of the vessel carrier, and the steering vectors are incomplete in these directions. Owing to the virtual transformation, the sensors in the virtual linear array will be unable to maintain uniformity, which does not favor the application of the ESPRIT-type methods. An aperture segmentation method can effectively overcome this problem. The U-shaped array is divided into two subarrays for different incident intervals to maximize the utilization of the array aperture and to ensure the integrity of the steering vectors, i.e., the left subarray corresponds to signals from [–90° 0°] and the right subarray corresponds to signals from [0° 90°]. Thus, there is always a subarray for any direction and the sensors are all capable of receiving signals. However, in the aperture segmentation method, the aperture of the virtual array is smaller than that of the receiving array at [–20° 20°].

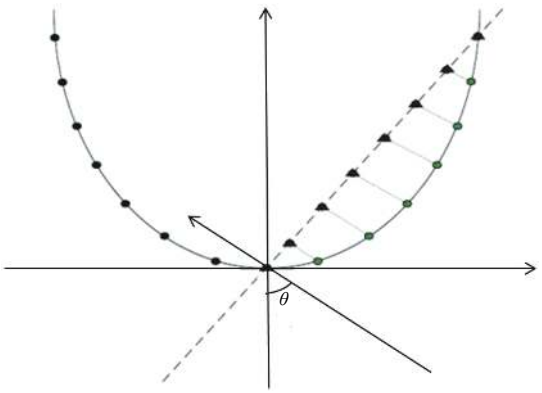

Fig. 2. Geometric position diagram of the U-shaped receiving array and the virtual linear array. The circles on the solid line indicate the real receiving array, and the triangles on the dashed line indicate the virtual array.

In order to perform the virtual transformation based on the U-shaped array, we first need to estimate the incident angle $\tilde{\theta}$, select the corresponding subarray, and determine the angle set Q_h. The virtual transformation technique is then applied based on this subarray. The virtual ULA with a sensor spacing equal to $\lambda/2$ is located on a line that connects the origin of the coordinates and the edge sensor in the subarray. The number of sensors in the virtual array is determined to minimize the discrepancies between the beam patterns of the real and virtual arrays, but it must not exceed the range of the maximum phase mode excited by the real array. It should be noted that the number of sensors in the virtual array does not need to match that in the real array.

As an example, the source frequency may be 165 kHz, the incident angle $\theta = 30^{\circ}$, and the acoustic speed is 1 500 m/s, and the sensors in the subarray corresponding to the incident signal are marked by the green circles in Fig. 2. The sensors in the virtual ULA are shown by the red triangles where the first is located at the origin. The incident angle $\tilde{\theta}$ can be estimated by beamforming on the subarray. The angle sector is selected as $Q = [\ \tilde{\theta} - \Delta\theta \quad \tilde{\theta} + \Delta\theta\ ]$, where $\Delta\theta = 5^{\circ}$or10°, and 100 equidistant angles that span this sector are used. The beam patterns for the real and virtual arrays are shown in Fig. 3, where the black solid line indicates the original beam pattern and the red dashed line is the virtual beam pattern. Clearly, the differences in the beam patterns before and after the virtual transformation are very small and they are basically consistent, which demonstrates the efficiency of the virtual transformation for the U-shaped array.

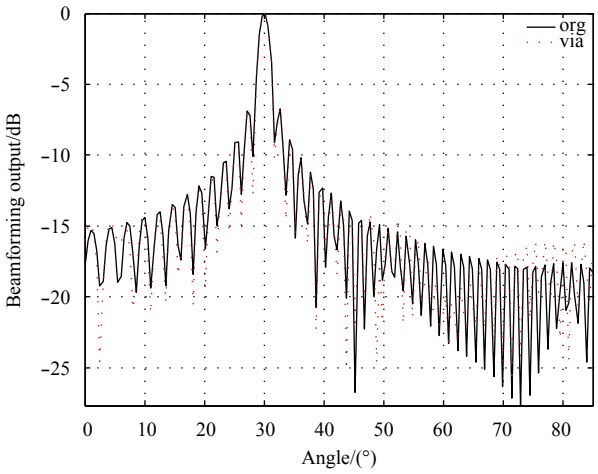

Fig. 3. Beam patterns of the real and virtual arrays. The black solid and red dashed lines indicate the real and virtual arrays, respectively.

3.3 *HRBD algorithm in the MBES system*

The implementation of HRBD in the proposed MBES system for the beamforming outputs and sensor outputs from every time slice can be summarized as follows.

(1) Estimate the angle range of the receiving signals and determine the corresponding subarray. Choose an angle sector Q_h and determine the structure of the virtual ULA and the corresponding transformation matrices $\{\boldsymbol{B}_h\}$, which are pre-computed off-line.

(2) Obtain the sensor output vector $\boldsymbol{y}_{\mathrm{v}}$ for the virtual ULA with $\boldsymbol{y}_{\mathrm{v}} = \boldsymbol{B}_h\boldsymbol{y}$, where $\boldsymbol{y}$ is the sensor output vector from the subarray. If necessary, estimate the number of sources K.

(3) Choose L angles $\bar{\theta}_l,\ l = 1, \ldots, L$ in the angle sector Q_h as the beam pointing angles and separate the virtual ULA into N_{v} subarrays.

(4) Operate TLS-ESPRIT-SB as before and then obtain the estimated DOA.

(5) Apply motion compensation to the estimated DOA and calculate the estimated TOA.

4 Computer simulation and experimental data processing results

4.1 *Computer simulation*

To assess the performance of the ESPRIT-SB for a U-shaped array (which we denote as via-ESPRIT-SB), we considered an example of DOA estimation using the TLS versions of both via-ESPRIT (we denote the ESPRIT with the virtual array transformation as via-ESPRIT) and via-ESPRIT-SB. The number of sources was assumed to be known where the individual source processes were uncorrelated and corrupted by white Gaussian noise. The simulation was evaluated based on 1 000 Monte-Carlo runs.

Two equal-power incident signals came from $\theta_1 = 34.6^{\circ}$ and $\theta_2 = 36.8^{\circ}$. For the via-ESPRIT-SB, we divided the virtual ULA in-

to $N(=4)$ subarrays with $P(=49)$ sensors, where each was equally separated by $5d$ and three given-pointing beams were formed. For the via-ESPRIT, the virtual ULA was divided into two subarrays, where each had 63 sensors and they were equally separated by d. Thirty snapshots were used for both algorithms.

Average root mean squared errors (RMSE) for all of the sources are plotted as a function of the signal-to-noise ratio (SNR) in Fig. 4. When the SNR approached –15 dB, the RMSE approached the variance of a uniform random variable (Van Trees, 2002). As expected, the RMSE exhibited a threshold behavior, where it increased dramatically below some SNR due to ambiguity sidelobes (Van Trees, 2002). A SNR gain in the order of $10\log P$ was clearly obtained, where the via-ESPRIT entered the threshold region earlier and the via-ESPRIT-SB performed better in the high SNR region.

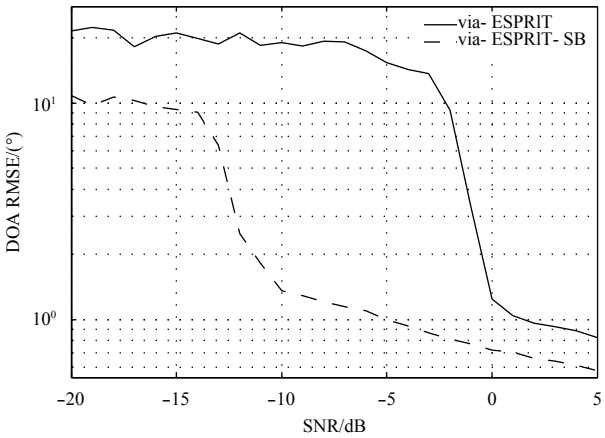

Fig. 4. Averaged RMSE in the DOA versus SNR for two equal-power signals from 34.6° and 36.8°. The solid line denotes the results obtained using the via-ESPRIT and the dashed line is those with the via-ESPRIT-SB.

Clearly, the virtual transformation performed efficiently when operating high resolution methods on a U-shaped array. The performance of the via-ESPRIT-SB was much better with a few snapshots compared with that of the via-ESPRIT for the following two reasons. First, the subarray configurations changed the performance where the via-ESPRIT-SB could increase the separation among the subarrays without any prior information to improve the performance. Second, the beamforming processing in the via-ESPRIT-SB could obtain a SNR gain and lower the threshold. Therefore, the via-ESPRIT-SB is more suitable for use in practical applications with a nonlinear array.

4.2 *Experimental data processing results*

An experiment was performed in the Qiandao Lake of Hangzhou, China. The bottom of this lake has a bowl shape and the depth decreases gradually from the edge to the middle of the lake, where it changes from about 10 to 60 m. The MBES system was installed underwater at a depth of 3 m in the well of a ship and the ship was anchored far off the shore. The system could be rotated 180° in the horizontal plane. The transmitting frequency was 165 kHz and the transmitting pulse width was 0.5 ms. The sample frequency for receiving was 4/3 times the transmitting frequency (Xu et al., 2009). Each record file comprised the receiving data according to one emission that included six pings. The MBES system formed 290 uniform receiving beams spanning from –85° to 85°. We assumed that the acoustic speed was a simple, fixed value such as 1 500 m/s.

The receiving signals were demodulated and a sampling rate for the baseband signal was 20 kHz. The results obtained by conventional beamforming processing using the baseband signal for one ping are shown in Fig. 5, where the abscissa is the beam angle and the ordinate is the number of snapshots. The value in the color bar denotes the quantization value of the energy after beamforming. The darker colored spots show the rough contours of the bottom. The BDI and the HRBD were applied to the beamforming outputs. A threshold of three was selected, so a signal with an energy three times higher than the average energy in this beam (the SNR was about 5 dB) was detected as the bottom signal. The estimates of the bottom obtained by the two methods are plotted in Figs 6a and b. In Fig. 6, the abscissa is the number of snapshots, where it corresponds to the TOA from the bottom, and the ordinate is the beam angle. The major differences between Figs 6a and 6b are in terms of the normal and oblique incident angles. In brief, at [–20° 20°], the data obtained by the whole array of sensors were used by the BDI, but only data from half the array of sensors were used for the virtual array transformation by the HRBD. The aperture of the array determines the resolution of beam forming and the number of array elements is related to the array gain. The results show that the HRBD obtained fewer hits than the BDI (Fig. 6). Thus, the performance of the HRBD was poorer in the case of normal incidence. At [–85° –70°] and [70° 85°], the hits in Fig. 6b formed a better trace than those in Fig. 6a, and the difference was even more significant in Fig. 7. Figure 7 shows the depth estimated based on the hits from three pings after bottom detection, where it was assumed that the acoustic speed was fixed, and the red and the black indicate the results obtained by the BDI and the HRBD, respectively. The estimated depths were the original results without the elimination of outliers and curve fitting. The left of Fig. 7 shows that when the range was more than 50 m, the beam angle was larger than 70°. The BDI missed the lake bottom whereas the HRBD continued following. The right of Fig. 7 shows that when the range was more than 150 m, the beam angle was larger than 75°. In addition, the depth in another direction is shown in Fig. 8 where the MBES was rotated nearly 100°. According to Fig. 8, there were two differences between the results obtained by the two algorithms: the results obtained by the HRBD were on the either side of the graph and the variance of the results obtained by the BDI was larger than that of the HRBD results, where both were caused by the higher resolution of the HRBD. When the beam angle was larger, the footprint area was wider and the resolution of the BDI was

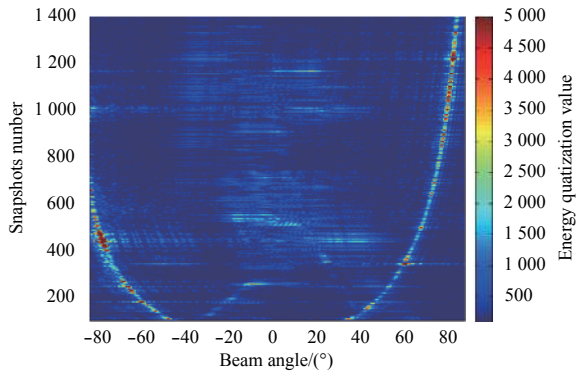

Fig. 5. Beamforming outputs at 165 kHz. The color bar indicates the quantization value of the energy after beamforming.

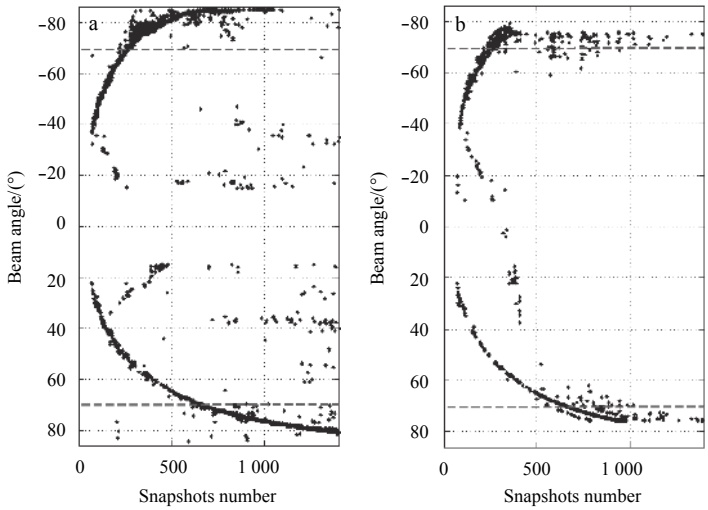

Fig. 6. The bottom detection results obtained with the BDI and the HRBD based on one ping. a. Hits using the HRBD, and b. hits using the BDI. The two dashed red lines indicate the beginning of the major differences between the hits using the HRBD and the BDI.

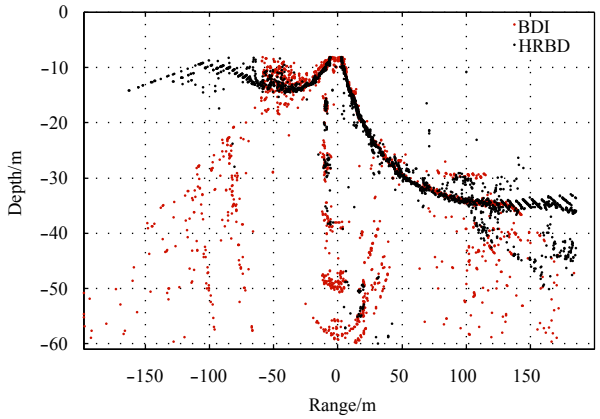

Fig. 7. The estimation of depth using the two methods based on three pings. The red indicates the results obtained by the BDI and the black by the HRBD.

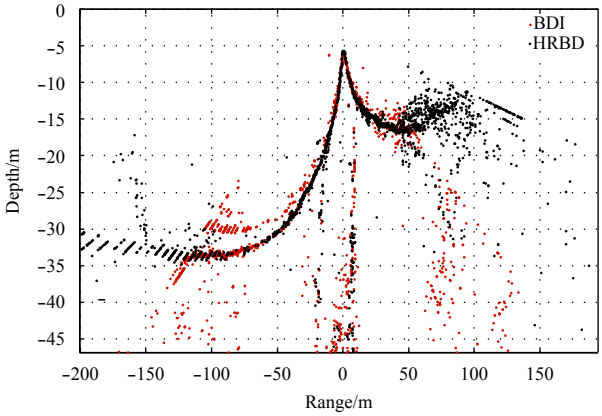

Fig. 8. The depth results obtained in the other direction. The red indicates the results obtained by the BDI and the black by the HRBD.

lower, and thus the variance of the hits was greater with the BDI. As shown in Fig. 5, the footprint spanned nearly 3° with 1 000 snapshots and the depth results obtained by the BDI ranged over more than 5 m. The HRBD followed the bottom better and the range was more than 50 m on both sides. In the edge region, the HRBD had a greater capacity for terrain following.

In summary, the performance of the HRBD in the normal incident area was poorer than that of the BDI due to the employment of aperture segmentation. However, on the edges of the beams, the HRBD could estimate the DOAs better and provide more details of the bottom depth. The HRBD method is more sensitive to the SNR, thereby leading to more false hits, and more accurate discrimination of outliers is required. However, the false hits and outliers can be eliminated easily after depth tracking according to the depth information coherence.

5 Conclusions

In this study, we developed a HRBD algorithm for a nonlinear array in the MBES systems, where we employed the ESPRIT with multiple-angle subarray beamforming and virtual array transformation. The proposed approach is an ESPRIT-type method so it is more flexible in terms of the array configuration, where it works better with few snapshots and a low SNR. Our simulations and experimental data processing results show that the proposed approach is particularly useful for a U-shaped array with few data snapshots and it can provide higher resolution on the edge of the swath.

References

Bourguignon S, Berger L, Scalabrin C, et al. 2009. Methodological developments for improved bottom detection with the ME70 multibeam echosounder. ICES Journal of Marine Science, 66(6): 1015–1022

Friedlander B, Weiss A J. 1992. Direction finding using spatial smoothing with interpolated arrays. IEEE Transactions on Aerospace and Electronic Systems, 28(2): 574–586

Jiang Ying. 2011. High resolution bottom detection for multi-beam echo sounder: Algorithm study and system implementation (in Chinese)[dissertation]. Hangzhou: Zhejiang University

Llort G, Sintes C. 2004. Improvement of multibeam echosondeur bottom detection. In: Proceedings of the SPIE Volume 5434, Multisensor, Multisource Information Fusion: Architectures, Algorithms, and Applications 2004. Orlando, FL, US: SPIE, 5434: 391–399

Roy R, Kailath T. 1989. ESPRIT-estimation of signal parameters via rotational invariance techniques. IEEE Transactions on Acoustics, Speech, and Signal Processing, 37(7): 984–995

Van Trees H L. 2002. Optimum Array Processing: Part IV of Detection, Estimation, and Modulation Theory. New York: Wiley

Weiss A J, Gavish M. 1991. Direction finding using ESPRIT with interpolated arrays. IEEE Transactions on Signal Processing, 39(6): 1473–1478

Xu Wen, Jiang Ying, Zhang Huiquan. 2012. ESPRIT with multiple-angle subarray beamforming. In: EURASIP Journal on Advances in Signal Processing, 2012(1): 152

Xu Wen, Xia Menglu, Chen Qizhang. 2009. True time-delay bandpass beamforming: A new implementation. In: OCEANS 2009-EUROPE. Bremen: IEEE, 1–5

Yang L, Taxt T. 1997. Multibeam sonar bottom detection using multiple subarrays. In: OCEANS '97. MTS/IEEE Conference Proceedings. Halifax, NS: IEEE, 2: 932–938